Frustration-driven magnetic order in hexagonal $InMnO_3$

X. Fabrèges,[1,2] I. Mirebeau,[1] S. Petit,[1] P. Bonville,[3] and A. A. Belik[4]

[1]*CEA, Centre de Saclay, /DSM/IRAMIS/ Laboratoire Léon Brillouin, F-91191 Gif-sur-Yvette, France*

[2]*Laboratoire National des Champs Magnétiques Intenses, CNRS-INSA-UJF-UPS, 143 Avenue de Rangueil, F-31400 Toulouse, France*

[3]*CEA, Centre de Saclay, /DSM/IRAMIS/ Service de Physique de l'Etat Condensé, F-91191 Gif-Sur-Yvette, France*

[4]*International Center for Materials Nanoarchitectonics (MANA), National Institute for Material Science (NIMS), 1-1 Namiki, Tsukuba, Ibaraki 305-0044, Japan*

(Received 18 May 2011; revised manuscript received 20 July 2011; published 15 August 2011)

$InMnO_3$ is a peculiar member of the hexagonal manganites h-$RMnO_3$ (where R is a rare-earth metal element), showing crystalline, electronic, and magnetic properties at variance with the other compounds of the family. We have studied high quality samples synthesized at high pressure and temperature by powder neutron diffraction. The position of the Mn ions is found to be close to the threshold $x = 1/3$ where superexchange Mn-Mn interactions along the c axis compensate. Magnetic long-range order occurs below $T_N = 120(2)$ K with a magnetic unit cell doubled along c, whereas short-range two-dimensional dynamical spin correlations are observed above T_N. We propose that pseudodipolar interactions are responsible for the long period magnetic structure.

DOI: 10.1103/PhysRevB.84.054455 PACS number(s): 75.25.−j, 61.05.fm, 76.80.+y, 75.30.Ds

I. INTRODUCTION

Multiferroic systems have been intensively studied in the past ten years as the coupling between ferroelectric and magnetic order parameters may lead to novel electronic devices. This coupling can have different microscopic origins, related either to Dzyaloshinskii-Moriya interactions[1,2] or to an exchange-striction mechanism, and it is still not fully understood. All multiferroics show complex and mostly noncollinear magnetic orders, arising from competing interactions and/or geometrical frustration.

The hexagonal $RMnO_3$ compounds (where R is a rare-earth metal element) provide textbook examples to study multiferroicity. Their crystal structure consists of triangular Mn planes packed along the c axis and separated by layers of rare-earth ions [R = Ho (Ref. 3)-Yb (Refs. 4 and 5)] or nonmagnetic ions such as Y (Ref. 6) or Sc.[7] Despite similar crystal structures, a rich variety of magnetic behaviors is observed versus temperature[8–10] and/or magnetic field,[11,12] pointing out the complexity of magnetic[13] and spin/lattice[14] interactions in such systems.

As shown recently,[15] the magnetic frustration does not arise only from the triangular geometry of antiferromagnetic (AF) first-neighbor interactions in the ab plane, but from competing interactions between Mn of adjacent planes. In all compounds, the Mn moments order within a triangular plane in a three sublattice Néel structure, corresponding to 120° arrangements of the Mn moments in a triangle. Four possible AF structures can be stabilized, described by irreducible representations of the $P6_3cm$ space group with $\mathbf{k} = \mathbf{0}$ propagation vector.[16] These structures differ by the orientations of the Mn moments with respect to the a,b crystal axes and by the relative orientations of Mn moments in adjacent planes. As shown in Ref. 15, the selection of a given structure is controlled by the Mn position in the unit cell, which depends on a unique parameter x for the 6c sites. The x value with respect to a critical threshold $x_0 = 1/3$ tunes the sign of the effective interaction between adjacent Mn planes. Within this framework, one can correlate the type of magnetic structure, the Mn position, and the sign of the effective exchange coupling in the compounds of the $RMnO_3$ family.

$InMnO_3$ is the only compound that does not fit simply with the above scheme. Actually, it corresponds to the peculiar situation where the Mn position is very close to $x_0 = 1/3$, so that interactions between adjacent Mn planes nearly cancel. Therefore one could expect new types of magnetic orders with two-dimensional behavior or stabilized by further neighbor interactions. Moreover, the $InMnO_3$ crystal structure has the smallest lattice constant a and the largest lattice constant c of the series,[17] so that in-plane and out-of-plane interactions differ much more than in the other compounds. The pioneering measurements of Greedan *et al.*[17] showed that the magnetic structure of $InMnO_3$ indeed differs from those of the whole series, with a $\mathbf{k} = (0\ 0\ \frac{1}{2})$ propagation vector, corresponding to a doubled periodicity along c. The sample showed broad magnetic reflections so that a two-dimensional order was postulated.

$InMnO_3$ is also interesting for its magnetoelectric properties. Ferroelectric hysteresis loop measurements performed on high quality samples showed no hysteresis below 250 K, establishing that the pure compound is actually not ferroelectric,[18] although ferroelectricity was earlier reported[19] in some samples below 500 K. In the pure samples, low-frequency permittivity exhibits an anomaly near T_N, showing evidence for a magnetoelectric coupling. Studies of Fe-substituted $InMnO_3$ showed that these compounds might constitute a new class of nearly room-temperature multiferroics.[20] In $InMnO_3$, the electronic structure of the In^{3+} ion with a fully filled 4d shell excludes the d_0-ness ferroelectricity at play in $YMnO_3$.[21] Considering the peculiar case of $InMnO_3$, a new covalent bonding mechanism was recently proposed to mediate ferroelectricity in hexagonal multiferroics.[22]

Since the measurements of Greedan *et al.*, no neutron study was made on $InMnO_3$. This could be due to the difficulty to synthesize big samples of high purity, and to the high absorption and low scattering power of the In^{3+} ion, which complicate the measurements. To shed more light on the peculiar behavior of $InMnO_3$, we have synthesized powder

sample of high purity in large amount under high-pressure and high-temperature conditions.[18] We performed high-resolution neutron study of the crystal structure versus temperature. We studied the magnetic order precisely by combining neutron-diffraction and Mössbauer spectroscopy in a ^{57}Fe-doped sample, and obtained the first results about the magnetic fluctuations. We determine the magnetic structure precisely using group theory and we propose a possible explanation for its origin based on the influence of pseudodipolar interactions.

II. EXPERIMENTAL DETAILS

Two samples were synthesized under high pressure. The first one is a stochiometric $InMnO_3$ sample of about 8 g used for the neutron measurements. A second sample of 0.5 g with chemical formula $InMn_{0.99}{}^{57}Fe_{0.01}O_3$ was prepared for the Mössbauer measurements. For the synthesis, appropriate mixtures of In_2O_3 (99.9% purity) and Mn_2O_3 and Fe_2O_3 were placed in Au capsules and treated at 5 GPa in a belt-type high-pressure apparatus at 1500 K for 90 min (heating rate 120 K/min). After the heat treatment, the samples were quenched to room temperature, and the pressure was slowly released. The resultant samples were dense black pellets. X-ray-diffraction measurements showed that they contained a small amount (1 mass %) of cubic In_2O_3 impurity.

The crystal structure and the evolution of the atomic parameter x with temperature were determined by measuring a neutron powder-diffraction (NPD) pattern at 300 K and at selected temperatures on the high-resolution powder diffractometer 3T2 of the Laboratoire Léon Brillouin (LLB) at Orphée reactor, with an incident neutron wavelength $\lambda = 1.2253$ Å. The magnetic structure was studied by collecting NPD patterns at several temperatures, between 200 K (above the magnetic transition) and 1.5 K. Both crystal and magnetic structures were refined using the FULLPROF suite.[23] The ^{57}Fe Mössbauer absorption spectra were recorded in the temperature range 4.2–140 K. We used a commercial ^{57}Co:Rh γ-ray source, mounted on a triangular velocity electromagnetic drive.

III. CRYSTAL STRUCTURE

The refined NPD pattern at 300 K is shown in Fig. 1. All Bragg reflexions of the pattern can be indexed within the hexagonal space group $P6_3cm$ with a peak width limited by the resolution. The lattice constants $a = 5.8837(1)$ Å and $c = 11.4829(1)$ Å at 300 K are in perfect agreement with previous results.[17,18] As noticed earlier, they strongly differ from those of the hexagonal $RMnO_3$ series, which scale from one compound to another.[24,25]

The refined atomic positions reported in Table I agree with previous determinations from x-ray diffraction.[17,18] They are very close to those determined in compounds of similar ionic radius (R = Ho, Y, Yb). Each Mn atom is surrounded by oxygen ions forming a MnO_5 bipyramidal structure, with three O (two O_4 and one O_3) ions close to the Mn plane, and two O (O_1 and O_2) ions at the apexes. Corner sharing MnO_5 bipyramids form layers separated along the c axis by In layers in which In ions occupy two distinct crystallographic sites (labeled 2a and 4b).

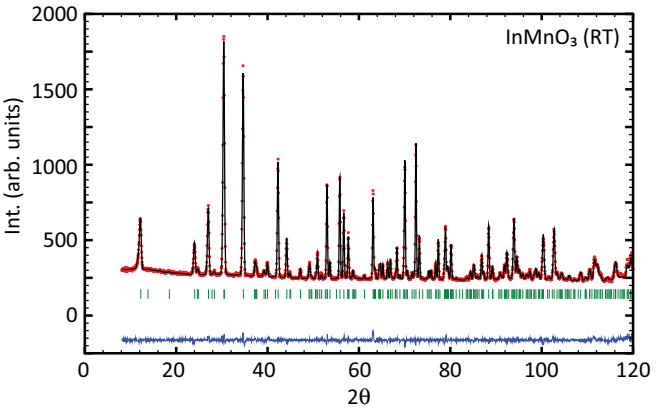

FIG. 1. (Color online) Observed and FULLPROF calculated NPD pattern at room temperature. The Bragg reflections (tics) and the difference between the observed and calculated patterns are plotted at the bottom.

The thermal variation of the positional parameter x of the Mn sites is reported in Fig. 2. One notices that x decreases with decreasing temperature down to about 150 K, then becomes very close to 1/3 in the $0 < T < 150$ K temperature range, which spans the whole ordered magnetic phase ($T_N = 118$ K). Based on this sole observation it is possible to predict that the two possible interplane exchange paths between Mn ions are almost identical (Fig. 3), which should dramatically decrease the effective exchange coupling along the c axis.

IV. MAGNETIC STRUCTURE

The NPD pattern collected at $T = 1.5$ K on the high-resolution diffractometer 3T2 is reported in Fig. 4 (bottom), focusing on the range in the scattering angle 2θ where magnetic Bragg reflections with half integer l values can be observed. All magnetic peaks can be indexed within the hexagonal space group $P6_3cm$ with a propagation vector $\mathbf{k} = [0\ 0\ \ 0.50(1)]$. In contrast with the other members of the family, there is no magnetic contribution at the positions of the structural peaks. The $(1\ 0\ \frac{2l+1}{2})$ Bragg reflections appear below $T_N = 120(2)$ K, with a peak width 20% above the experimental resolution and their thermal variation is monotonic (Fig. 4, top). When taking the instrumental resolution into account, we find that the intrinsic broadening of the magnetic reflections is identical

TABLE I. Atom positions, thermal parameters, and discrepancy factors at room temperature.

Atoms	x	y	z	B_{iso}
In (2a)	0	0	0.274(2)	0.845(120)
In (4b)	$\frac{1}{3}$	$\frac{2}{3}$	0.232(2)	0.490(65)
Mn (6c)	0.345(4)	0	0	0.334(43)
O_1 (6c)	0.307(2)	0	0.165(3)	0.686(16)
O_2 (6c)	0.640(1)	0	0.336(3)	0.686(16)
O_3 (4b)	0	0	0.475(2)	0.954(100)
O_4 (2a)	$\frac{1}{3}$	$\frac{2}{3}$	0.020(2)	0.575(54)
Discrepancy factors	Bragg R factor	4.32%		
	R_F factor	3.21%		

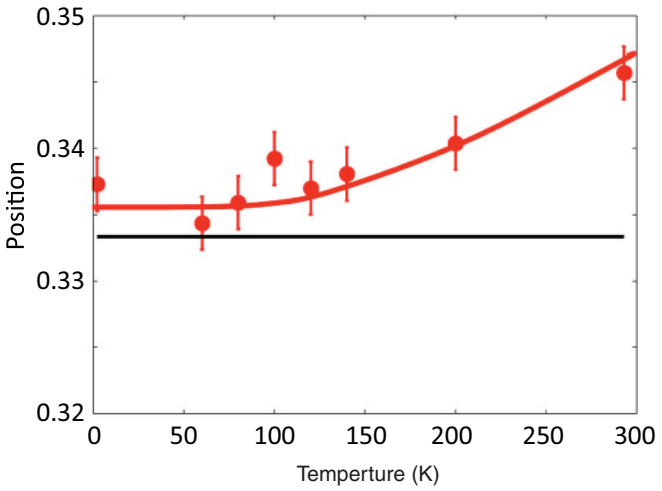

FIG. 2. (Color online) Refined position x of Mn versus temperature in reduced units of the cell parameter a. The horizontal black line is located at $x = 1/3$, the red line is a guide to the eyes.

for all magnetic peaks and corresponds to a $3d$ magnetic correlation length of about 200 Å at low temperature. This isotropic and constant broadening contrasts with the observations of Ref. 17, where $2d$ and $3d$ correlations were found to coexist below T_N. The difference may be related to the different sample preparations. All these observation show the onset below $T_N = 120(2)$ K of a three-dimensional order for the Mn moments, with a magnetic unit cell doubled along the c axis, and without spin reorientation transition below T_N.

To analyze the magnetic structure we searched for all irreductible representations (IR) compatible with the crystal symmetry using the theory of group representation analysis[26] and the program BASIREPS.[27] The atomic position of Mn ions in

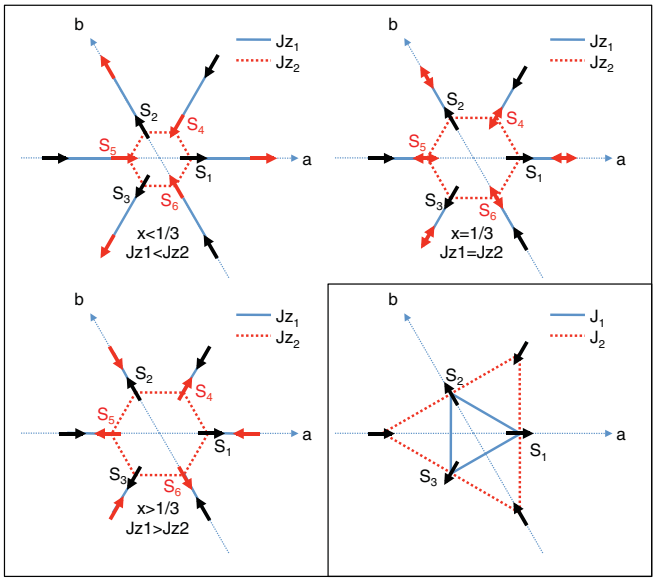

FIG. 3. (Color online) Interplane exchange paths versus Mn position. Two exchange paths Jz_1 and Jz_2 are in competition and the $x = 1/3$ Mn position corresponds to the specific case $Jz_1 = Jz_2$. Inset: in-plane exchange paths leading to the 120° magnetic configuration.

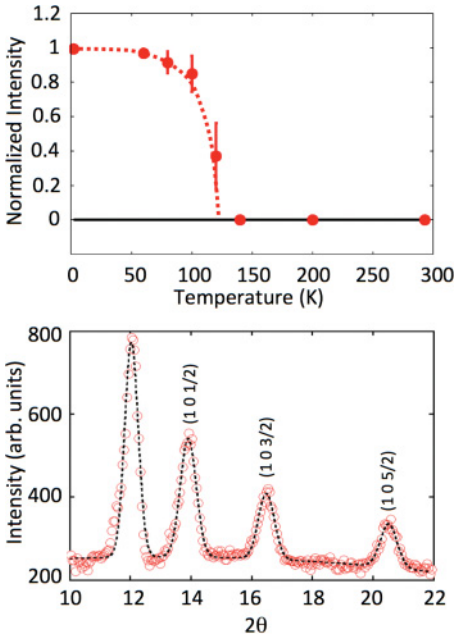

FIG. 4. (Color online) Upper panel: integrated intensity of the (1 0 1/2) Bragg reflection versus temperature. The red dashed line is a guide to the eyes. Lower panel: observed NPD pattern at low temperature ($T = 1.5$ K). The $\mathbf{k} = (0\ 0\ \frac{1}{2})$ propagation vector is easily observed through the existence of $(1\ 0\ \frac{(l+1)}{2})$ Bragg reflections.

the unit cell was kept equal to (1/3 0 0), close to the position observed experimentally. In the space group $P6_3cm$, the $6c$ site of Mn ions allows six irreductible representations labeled from Γ_1 to Γ_6. The Γ_1 and Γ_4 representations are defined by one basis vector associated with a 120° magnetic order within the ab planes whereas the Γ_2 and Γ_3 are defined by two basis vectors, the second one allowing an out-of-plane component. The Γ_5 and Γ_6 representations correspond to magnetic orders with unequivalent magnetic moments on each site, which have not been considered, as for the rest of the RMnO$_3$ family.[16]

The Fourier component corresponding to the propagation vector $\mathbf{k}$ for a Mn site n of the unit cell is expressed as $M_n(z) = M\, e^{-i\mathbf{k}\cdot\mathbf{r}_n}$ where r_n denotes the position of the nth Mn ion in the unit cell, referred by its z coordinate along the c axis. In our particular case, the $\mathbf{k} = (0\ 0\ \frac{1}{2})$ propagation vector yields a purely real Fourier component of the magnetic moment in the $z = 0, 1, 2,...$ Mn planes and purely imaginary components in the $z = 1/2, 3/2,...$planes (Fig. 5). In order to overcome this difficulty and to be consistent with the presence of equivalent moments on all Mn sites deduced from the Mössbauer results (see below), we have introduced a global phase shift $\phi = 2\pi/8$ in the expression of the structure factor. The phase and amplitude of the Fourier components were used to determine the magnitude of the ordered moment at a given Mn site.

As for the rest of the RMnO$_3$ family, we find that magnetic configurations associated to Γ_1 and Γ_3 IR are homometric (namely, they share the same structure factor) so they cannot be distinguished in a powder neutron-diffraction experiment. The same holds for the Γ_2 and Γ_4 magnetic configurations. Our refinements yield a discrepancy factor $R_{mag} = 12.54\%$ for the Γ_2 and Γ_4 IR, much better than for Γ_1 and Γ_3 ($R_{mag} = 19.8\%$). The R_{Bragg} factor in the ordered magnetic

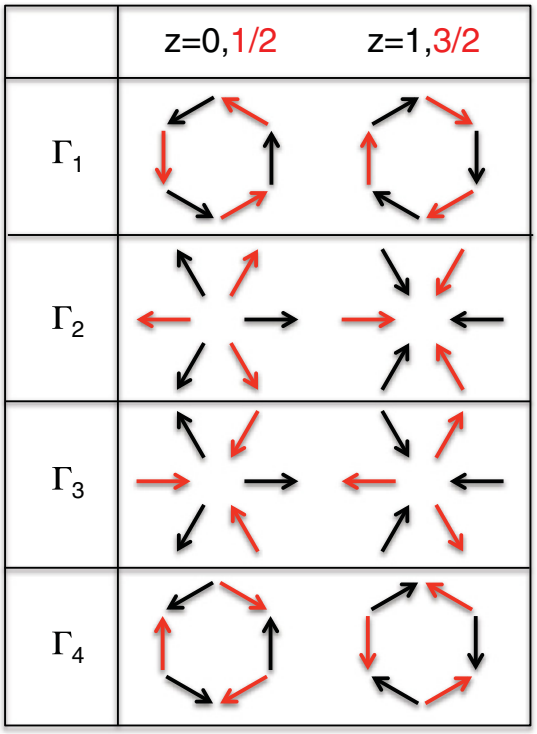

FIG. 5. (Color online) Magnetic structures associated to the four unidimensional irreductible representations of the $P6_3cm$ space group. Red arrows indicate magnetic moments with real Fourier components, black arrows indicate moments with imaginary Fourier components.

phase was close to 5%. The best fit of our data was obtained for an ordered magnetic moment of $3.25\mu_B$ at 1.5 K, very similar to the moment found in the rest of the hexagonal RMnO$_3$ family.[16] We conclude that the Mn moments order in the a,b planes, in bilayers ordered according to either a Γ_2 or a Γ_4 configuration, as for YbMnO$_3$ or ScMnO$_3$ with $\mathbf{k} = \mathbf{0}$ propagation vector, but with antiferromagnetic relative orientations of two neighboring bilayers.

V. ^{57}Fe MÖSSBAUER DATA

Three ^{57}Fe Mössbauer spectra were recorded, at $T = 140$, 80, and 4.2 K. The spectra at 4.2 and 140 K are represented in Fig. 6. At 140 K, a quadrupolar hyperfine spectrum is observed, with a quadrupolar splitting $|\Delta E_Q| = 0.5(1)$ mm/s, typical for Fe^{3+} in the paramagnetic phase. Below T_N, at 4.2 and 80 K, a six-line spectrum is observed, attributable to a single magnetic hyperfine field, with a small quadrupolar shift $\epsilon = 0.26(1)$ mm/s. This indicates that all the ^{57}Fe nuclei experience the same hyperfine field (48.6 T at 4.2 K and 43 T at 80 K), hence all the substituted Fe ions bear the same magnetic moment. One can conclude that the ordered magnetic moment of the Mn ion is the same on each site.

It is possible to obtain information about the angle θ between the hyperfine field and the principal axis of the electric-field gradient (EFG) tensor, responsible for the quadrupolar hyperfine interaction. Indeed, the relationship between the quadrupolar splitting obtained in the paramagnetic phase and the quadrupolar shift measured in the magnetically ordered

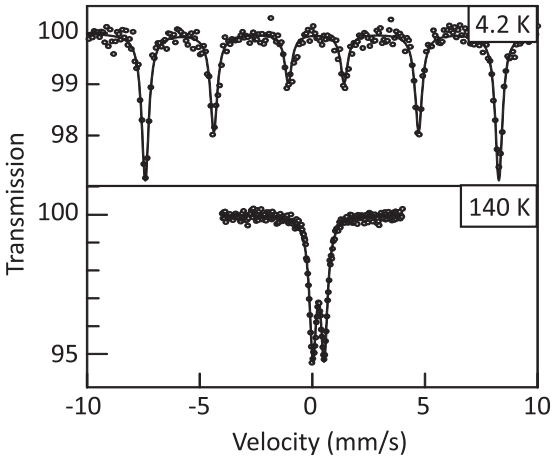

FIG. 6. ^{57}Fe Mössbauer spectra in InMn$_{0.99}$Fe$_{0.01}$O$_3$ below and above $T_N = 120$ K. At $T = 140$ K a quadrupolar doublet characteristic of paramagnetic Fe^{3+} is observed. At $T = 4.2$ K the spectrum shows a six-lines hyperfine pattern perfectly reproduced by a single hyperfine magnetic field.

phase is $\epsilon = \Delta E_Q \frac{3\cos^2\theta - 1}{2}$. Since the sign of ΔE_Q cannot be determined, one derives two acceptable values for θ: 90° and 35.3°. The local symmetry of the Fe(Mn) sites is 6c, which implies that the EFG tensor has one axis along **c** and the two other axes in the a,b plane, but the principal axis cannot be determined only by symmetry considerations. Assuming it lies along **c**, then the solution $\theta = 90°$ would be adequate, in analogy with the rest of the RMnO$_3$ family.

VI. SHORT-RANGE CORRELATIONS IN THE PARAMAGNETIC PHASE

The powder-diffraction patterns measured on 3T2 above T_N (Fig. 7) show a strong diffuse scattering, already observed by Greedan *et al.*[17] The asymmetric shape of this scattering is directly connected with the presence of two-dimensional correlations between Mn moments of a given plane. Using a Warren-like profile[28] we refined the length scale ξ of these correlations (Fig. 8). The ξ values above T_N agree with those deduced previously.[17] However, in the sample studied in Ref. 17, the $2d$ correlations persist below T_N, coexisting with half integer Bragg reflections of finite width, whereas in the present case ξ diverges at T_N, showing the onset of a purely three-dimensional long-range magnetic order.

Interestingly, spectra collected in the same temperature range on the G6.1 diffractometer using a large incident neutron wavelength showed no signature of this diffuse scattering (Fig. 7, bottom). To understand this peculiarity, one should notice that a neutron diffractometer probes both elastic and inelastic signals and integrates all contributions at a given scattering angle. The energy range over which this integration is performed depends on the energy of the incident neutron. Knowing that G6.1 is a cold diffractometer with an incident energy $\hbar^2 k_i^2 = 4$ meV ($\lambda = 4.74$ Å) and 3T2 a thermal one with $\hbar^2 k_i^2 \approx 40$ meV ($\lambda = 1.225$ Å), one concludes that the observed diffuse scattering above T_N corresponds to dynamical short-range correlations between Mn moments, involving high-energy fluctuations, at a scale of tens of meV.

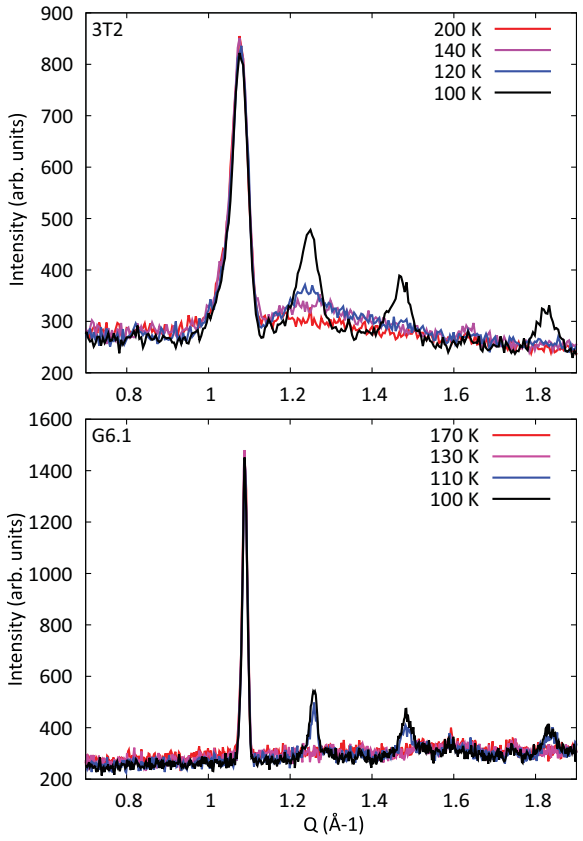

FIG. 7. (Color online) Observed and FULLPROF calculated NPD patterns at several temperatures. Above T_N a strong diffuse scattering is observed on the patterns recorded on 3T2 spectrometer (top) with $\lambda = 1.225$ Å. This scattering is not visible on the G6.1 patterns (bottom) for which $\lambda = 4.74$ Å.

The analysis of the paramagnetic scattering suggests a picture of uncorrelated Mn planes, in which dynamical magnetic correlations develop with decreasing temperature down to T_N. The $3d$ magnetic ordering stabilized at T_N should be triggered by a weak interaction between Mn moments belonging to different planes, whose origin is discussed below.

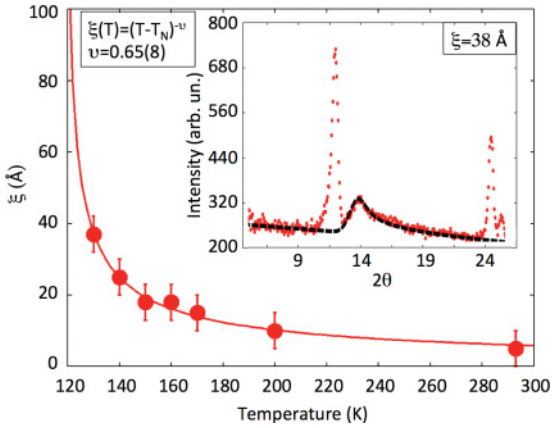

FIG. 8. (Color online) Refined correlation length versus temperature (red dots) and fit of the critical exponent ν (solid line). Inset: intensity recorded at $T = 130$ K on the 3T2 spectrometer. The dashed line is a fit of the diffuse intensity with a Warren function.

VII. DISCUSSION

A. Magnetic ordering and frustration

We first recall the scheme of interactions used in Ref. 15 to discuss the magnetic structures observed in the hexagonal $R\mathrm{MnO_3}$ family with $\mathbf{k} = \mathbf{0}$ propagation vector. In these compounds, a given magnetic structure of symmetry Γ_i ($i = 1$–4) is stabilized by near-neighbor exchange interactions as well as planar and uniaxial anisotropies, so that the Hamiltonian of the system is composed of three terms:

$$\mathcal{H}_{\mathrm{Heis}} = \sum_{i,j} J_{ij}\, \mathbf{S}_i.\mathbf{S}_j + \sum_i D\left(S_i^z\right)^2 - \sum_i \mathbf{h}_i.\mathbf{S}_i, \quad (1)$$

where S_i is the Mn spin on the ith site, J_{ij} is the exchange constant, D is a planar anisotropy, and $\mathbf{h}_i$ is a local field yielding a preferential orientation for the $\mathbf{S}_i$ spin.

The exchange term has two distinct parts, involving in-plane and out-of-plane interactions, respectively. Due to the triangular lattice, the in-plane interactions yield a two-dimensional 120° order, with no preferential orientation of the magnetic moments with respect to the crystal axes. Out-of-plane interactions couple Mn moments from adjacent planes yielding the $3d$ order. In this scenario, the Mn position is crucial since two possible exchange paths compete along the c axis. The selection of a given structure is controlled by the Mn position. In $\mathrm{InMnO_3}$, the Mn position is close to the critical threshold of $1/3$ for which the two exchange paths are strictly equal. This leads to a full compensation of the exchange interactions along the c axis and to an effective out-of-plane exchange interaction close to zero. This specific position of the Mn ions could explain the dynamical short-range $2d$ order observed above T_N, and attributed to uncorrelated Mn planes.

The two other terms of Eq. (1) are, respectively, the planar anisotropy D, which confines the Mn moments in the basal plane, and the local field $\mathbf{h}$, which plays the role of a uniaxial anisotropy and selects preferential directions either along or perpendicular to the crystal axes.

These terms, however, cannot explain the long period $3d$ structure with $\mathbf{k} = (0\ 0\ \frac{1}{2})$ stabilized in $\mathrm{InMnO_3}$. Therefore one needs to consider further neighbor interactions, with different symmetries than the exchange interactions, such as the Dzyaloshinskii-Moriya (DM) or the pseudodipolar interaction.[29] A similar approach[30] was proposed to account for the ordering of the Yb moments in $\mathrm{YbMnO_3}$. In the following, we focus on the pseudodipolar interaction since the DM interaction is hardly compatible with long exchange path (Mn-O-O-Mn and Mn-O-O-O-O-Mn) between Mn of different planes. The pseudodipolar interaction is written as

$$\mathcal{H}_{\mathrm{dip}} = -\sum_{i,j} \mathbf{S}_i\, J_{ij}^{\mathrm{dip}}\, \mathbf{S}_j$$

$$= -\alpha \sum_i \sum_j \left[3\frac{(\mathbf{S}_j.\mathbf{r}_{ij}).\mathbf{r}_{ij}}{r_{ij}^2} - \mathbf{S}_j \right] \mathbf{S}_i, \quad (2)$$

where α is a constant and $\mathbf{r}_{ij}$ joins sites i and j. The matricial representation of the pseudodipolar interaction J_{ij}^{dip} coupling two different Mn sites reads as

$$J_{ij}^{\mathrm{dip}} = \alpha \left[\frac{3}{r_{ij}^2} \begin{pmatrix} r_{ij}^x r_{ij}^x & r_{ij}^x r_{ij}^y & r_{ij}^x r_{ij}^z \\ r_{ij}^y r_{ij}^x & r_{ij}^y r_{ij}^y & r_{ij}^y r_{ij}^z \\ r_{ij}^z r_{ij}^x & r_{ij}^z r_{ij}^y & r_{ij}^z r_{ij}^z \end{pmatrix} - \mathbb{1} \right], \qquad (3)$$

where $\mathbb{1}$ is the identity matrix. Assuming the $\mathbf{k} = (0\ 0\ \frac{1}{2})$ magnetic structure described above, we calculate the magnetic field $\mathbf{B}_i$ induced on the ith site by the surrounding Mn at sites j, $\mathbf{B}_i = \sum_j J_{ij}^{\mathrm{dip}} \mathbf{S}_j$. First, we find that the contribution arising from the neighboring sites in adjacent $z = \pm 1/2$ planes is zero. Thus there is no pseudodipolar coupling between adjacent layers, in agreement with the idea of purely two-dimensional dynamical correlations above T_{N}. In contrast, the contribution from sites in $z = \pm 1$ planes is different from zero. Moreover, the classical energy calculated as $E = -\mathbf{B}_i \mathbf{S}_i$ is negative (assuming α is positive). In other words, the pseudodipolar interaction stabilizes the $3d$ magnetic structure observed in $InMnO_3$ and drives the $\mathbf{k} = (0\ 0\ \frac{1}{2})$ propagation vector.

It is commonly accepted that pseudodipolar interactions are weaker than exchange interactions by at least one order of magnitude. Therefore magnetic correlations along the c axis should be weaker in $InMnO_3$ than in the rest of the $RMnO_3$ family yielding smaller correlation lengths. This particularity could explain the difference observed in our experimental data between the nuclear and magnetic peak widths.

B. Spin-wave spectrum

To confirm the possible role of the pseudodipolar coupling, we propose to carry out spin dynamics measurements, as specific features associated to the pseudodipolar coupling should be easily seen on spin-wave dispersion relations. This issue could be sorted out by inelastic neutron-scattering experiments performed on a triple axis spectrometer.

From the interaction scheme described above, one can calculate the spectrum of the spin-wave excitations in the ordered phase. We use the previous Heisenberg Hamiltonian, to which we add the pseudodipolar term, written as

$$\mathcal{H} = \mathcal{H}_{\mathrm{Heis}} - \sum \mathbf{S}_i \, J_{ij}^{\mathrm{dip}} \, \mathbf{S}_j. \qquad (4)$$

Each term affects the spin-wave spectrum in a specific way. The Heisenberg Hamiltonian $\mathcal{H}_{\mathrm{Heis}}$ is responsible for the magnitude of the dispersion, namely the in-plane exchange interaction induces the dispersion along the $(q_h\ 0\ 0)$ and $(0\ q_k\ 0)$ directions of the reciprocal space, whereas the out-of-plane exchange yields the dispersion along the $(0\ 0\ q_l)$ direction. Considering that the exchange interactions along c nearly cancel due to the specific Mn position, one can predict that no dispersion should be observed along the $(0\ 0\ q_l)$ direction, yielding two flat modes. The anisotropy terms induce gaps in the dispersion curves. In $RMnO_3$, the planar anisotropy term induces a large gap of about 6 meV,[31] and the uniaxial term a smaller one, strongly dependent on temperature and likely enhanced by interaction with the rare-earth moment.[32]

As concerns the influence of the pseudodipolar term on the spin-wave spectrum, one notices that this term involves both diagonal and off-diagonal elements introducing new coupling between spin components. The diagonal elements act mainly as a combination of exchange and uniaxial anisotropy. Its effect should be easily seen at the zone center, the uniaxial gap increasing with the dipolar interaction strength α.

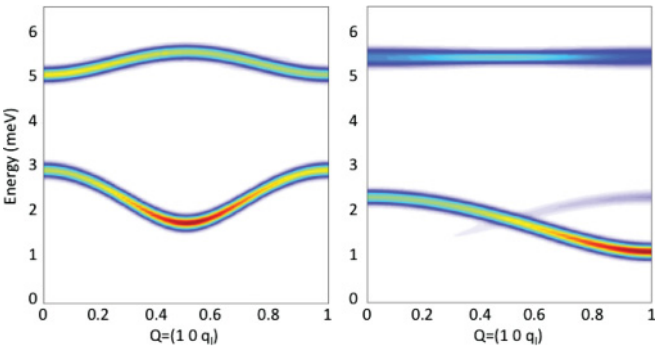

FIG. 9. (Color online) Left: numerical calculation of the dynamical structure factor of spin waves along the $(0\ 0\ q_l)$ direction in case of pseudodipolar coupling between Mn. Right: numerical calculation of the dynamical structure factor of spin waves along the $(0\ 0\ q_l)$ direction in the case of antiferromagnetic interplane exchange coupling between Mn.

To illustrate this point, spin-wave calculations of the dynamical structure factor were made with the following parameters: $J = 2.6$ meV, $D = 0.55$ meV and $h = 0.1$ meV in the case of the magnetic structure of $InMnO_3$ refined above. The results along the $(0\ 0\ q_l)$ direction of the reciprocal space are reported in Fig. 9 in the case of pseudodipolar (left) and interplane exchange (right) coupling. The coupling constant α and J_{inter} were taken equal to 0.01 meV (antiferromagnetic). In both cases, the spin-wave dispersion curves are characterized by two gaps around 5 and 2 meV induced, respectively, by D and h.

Considering the shape of the dispersion curves, the pseudodipolar interaction induces a dispersion of both the 2- and 5-meV modes. A maximum (respectively, minimum) is observed at $\mathbf{Q} = (1\ 0\ 0)$ and a minimum (respectively, maximum) is observed at $\mathbf{Q} = (1\ 0\ \frac{1}{2})$. On the other hand, the interplane exchange induces a dispersion of the low-energy mode with a maximum at $\mathbf{Q} = (1\ 0\ 0)$ and a minimum at $\mathbf{Q} = (1\ 0\ 1)$, whereas the 5-meV mode remains almost flat. The pseudodipolar interaction is at the origin of a change in the periodicity of the dispersion in perfect agreement with the $\mathbf{k} = (0\ 0\ \frac{1}{2})$ propagation vector.

Inelastic neutron scattering is mandatory to confirm the scheme of interaction proposed here for $InMnO_3$ as both behaviors are easily distinguishable and should be seen on a triple axis or time-of-flight spectrometer. Up to now, precise measurements were hampered by the low intensity given by the available samples and by the powder averaging, but we hope to perform them in future.

VIII. CONCLUSION

In conclusion, our experimental study of $InMnO_3$ by neutron powder diffraction and Mössbauer spectroscopy shows the onset of a three-dimensional magnetic order below $T_{\mathrm{N}} = 120(2)$ K. The magnetic order with $\mathbf{k} = (0\ 0\ \frac{1}{2})$ propagation vector shows a doubling of the magnetic unit cell along the c axis, in contrast with the other compounds of the

RMnO$_3$ family. This feature is directly related to the peculiar value of the Mn positional parameter in InMnO$_3$, close to the 1/3 threshold where the effective exchange interaction along the c axis cancels. We suggest that weak out-of-plane pseudodipolar Mn interactions are responsible for the long period of the magnetic order. This weak coupling together with the strong in-plane coupling yields the onset of two-dimensional correlations between fluctuating moments, which settle above T_N. InMnO$_3$ provides an original example of the links between magnetic frustration and multiferroicity, which should be further studied by inelastic neutron scattering.

ACKNOWLEDGMENTS

This work was partially supported by World Premier International Research Center (WPI) Initiative on Materials Nanoarchitectonics (MEXT, Japan), by the Japan Society for the Promotion of Science (JSPS) through its Funding Program for World-Leading Innovative R&D on Science and Technology (FIRST Program), and by the Grants-in-Aid for Scientific Research (Grant No. 22246083) from JSPS, Japan. We thank L. C. Chapon for his useful advice concerning the data treatment.

[1] H. Katsura, N. Nagaosa, and A. V. Balatsky, Phys. Rev. Lett. **95**, 057205 (2005).
[2] I. A. Sergienko and E. Dagotto, Phys. Rev. B **73**, 094434 (2006).
[3] S. Nandi, A. Kreyssig, L. Tan, J. W. Kim, J. Q. Yan, J. C. Lang, D. Haskel, R. J. McQueeney, and A. I. Goldman, Phys. Rev. Lett. **100**, 217201 (2008).
[4] M. Isobe, N. Kimizuka, M. Nakamura, and T. Mohri, Acta Crystallogr. Sect. C **47**, 423 (1991).
[5] H. A. Salama, G. A. Stewart, D. H. Ryan, M. Elouneg-Jamroz, and A. V. J. Edge, J. Phys.: Condens. Matter **20**, (2008).
[6] B. B. Van Aken, A. Meetsma, and T. T. M. Palstra, Acta Crystallogr. Sect. C **57**, 230 (2001).
[7] A. Munoz, J. A. Alonso, M. J. Martinez-Lope, M. T. Casais, J. L. Martinez, and M. T. Fernandez-Diaz, Chem. Mater. **13**, 1497 (2001).
[8] H. Sugie, N. Iwata, and K. Kohn, J. Phys. Soc. Jpn. **71**, 1558 (2002).
[9] B. B. Van Aken, T. T. M. Palstra, A. Filippetti, and N. A. Spaldin, Nat. Mater. **3**, 164 (2004).
[10] M. Bieringer and J. E. Greedan, J. Solid State Chem. **143**, 132 (1999).
[11] O. P. Vajk, M. Kenzelmann, J. W. Lynn, S. B. Kim, and S. W. Cheong, Phys. Rev. Lett. **94**, 087601 (2005).
[12] B. Lorenz, F. Yen, M. M. Gospodinov, and C. W. Chu, Phys. Rev. B **71**, 014438 (2005).
[13] P. J. Brown and T. Chatterji, J. Phys.: Condens. Matter **18**, 10085 (2006).
[14] C. dela Cruz, F. Yen, B. Lorenz, Y. Q. Wang, Y. Y. Sun, M. M. Gospodinov, and C. W. Chu, Phys. Rev. B **71**, 060407 (2005).
[15] X. Fabreges, S. Petit, I. Mirebeau, S. Pailhes, L. Pinsard, A. Forget, M. T. Fernandez-Diaz, and F. Porcher, Phys. Rev. Lett. **103**, 067204 (2009).
[16] A. Munoz, J. A. Alonso, M. J. Martinez-Lope, M. T. Casais, J. L. Martinez, and M. T. Fernandez-Diaz, Phys. Rev. B **62**, 9498 (2000).
[17] J. E. Greedan, M. Bieringer, J. F. Britten, D. M. Giaquinta, and H. C. Zurloye, J. Solid State Chem. **116**, 118 (1995).
[18] A. A. Belik, S. Kamba, M. Savinov, D. Nuzhnyy, M. Tachibana, E. Takayama-Muromachi, and V. Goian, Phys. Rev. B **79**, 054411 (2009).
[19] C. R. Serrao, S. B. Krupanidhi, J. Bhattacharjee, U. V. Waghmare, A. K. Kundu, and C. N. R. Rao, J. Appl. Phys. **100** (2006).
[20] A. A. Belik, T. Furubayashi, Y. Matsushita, M. Tanaka, S. Hishita, and E. Takayama-Muromachi, Angew. Chem. Int. Ed. **48**, 6117 (2009).
[21] D. Y. Cho *et al.*, Phys. Rev. Lett. **98**, 217601 (2007).
[22] M.-A. Oak, J.-H. Lee, H. M. Jang, J. S. Goh, H. J. Choi, and J. F. Scott, Phys. Rev. Lett. **106**, 047601 (2011).
[23] J. Rodriguez-Carvajal, Physica B **192**, 55 (1993).
[24] B. B. Van Aken, A. Meetsma, and T. T. M. Palstra, Acta Crystallogr. Sect. E **57**, i87 (2001).
[25] H. W. Xu, J. Iwasaki, T. Shimizu, H. Satoh, and N. Kamegashira, J. Alloys Compd. **221**, 274 (1995).
[26] E. F. Bertaut and M. Mercier, Phys. Lett. **5**, 27 (1963).
[27] J. Rodriguez-Carvajal [http://www.ill.eu/sites/fullprof/php/programsfa7c.html?pagina=GBasireps], (2001).
[28] B. E. Warren, Phys. Rev. **59**, 693 (1941).
[29] J. H. van Vleck, Phys. Rev. **52**, 1178 (1937).
[30] X. Fabreges, I. Mirebeau, P. Bonville, S. Petit, G. Lebras-Jasmin, A. Forget, G. Andre, and S. Pailhes, Phys. Rev. B **78**, 214422 (2008).
[31] S. Petit, F. Moussa, M. Hennion, S. Pailhes, L. Pinsard-Gaudart, and A. Ivanov, Phys. Rev. Lett. **99**, 266604 (2007).
[32] X. Fabreges, S. Petit, and I. Mirebeau (unpublished).